

The Low Effective Spin of Binary Black Holes and Implications for Individual Gravitational-Wave Events

SIMONA MILLER,¹ THOMAS A. CALLISTER,² AND WILL M. FARR^{2,3}

¹*Department of Physics, Smith College, Northampton, MA 01063, USA*

²*Center for Computational Astrophysics, Flatiron Institute, New York, NY 10010, USA*

³*Department of Physics and Astronomy, Stony Brook University, Stony Brook NY 11794, USA*

ABSTRACT

While the Advanced LIGO and Virgo gravitational-wave experiments now regularly observe binary black hole mergers, the evolutionary origin of these events remains a mystery. Analysis of the binary black hole spin distribution may shed light on this mystery, offering a means of discriminating between different binary formation channels. Using the data from Advanced LIGO and Virgo’s first and second observing runs, here we seek to carefully characterize the distribution of effective spin χ_{eff} among binary black holes, hierarchically measuring the distribution’s mean μ and variance σ^2 while accounting for selection effects and degeneracies between spin and other black hole parameters. We demonstrate that the known population of binary black holes have spins that are both small, with $\mu \approx 0$, and very narrowly distributed, with $\sigma^2 \leq 0.07$ at 95% credibility. We then explore what these ensemble properties imply about the spins of *individual* binary black hole mergers, re-analyzing existing gravitational-wave events with a population-informed prior on their effective spin. Under this analysis, the binary black hole GW170729, which previously excluded $\chi_{\text{eff}} = 0$, is now consistent with zero effective spin at $\sim 10\%$ credibility. More broadly, we find that uninformative spin priors generally yield *overestimates* for the effective spin magnitudes of compact binary mergers.

1. INTRODUCTION

In their first two observing runs, the Advanced LIGO (Laser Interferometer Gravitational-wave Observatory) and Advanced Virgo experiments (Aasi et al. 2015; Acernese et al. 2015) have detected gravitational waves from eleven compact binary coalescences - ten binary black hole (BBH) mergers and one binary neutron star (BNS) merger (Abbott et al. 2016a, 2017, 2019a). This early catalog of gravitational-wave (GW) signals has already been used to measure a diverse set of physical parameters, from the binaries’ component masses and spins (Abbott et al. 2016b, 2019b,a; Chatziioannou et al. 2019; Kimball et al. 2019) to more complex phenomena such as tidal effects (Abbott et al. 2018a; Raithel et al. 2018) and consistency with general relativity (Abbott et al. 2016c, 2019c,d).

The number of gravitational-wave detections is rapidly growing. Now roughly halfway through their third “O3” observing run, LIGO and Virgo have already reported ~ 40 new detection candidates; to-

gether with the newly-built KAGRA detector (Aso et al. 2013), they are expected to observe an additional ~ 100 events in O4 (Abbott et al. 2018b). As the number of gravitational-wave detections increases, we can shift our focus from the study of individual binaries to the analysis of their ensemble (Abbott et al. 2016a, 2019e). While the astrophysical details of compact binary evolution are only weakly reflected in the properties of individual events, we expect them to much more strongly inform binaries’ population properties – the distributions of component masses, spins, and redshifts. Uncovering these ensemble properties is therefore a promising means of determining which evolutionary channel drives the formation of compact binary mergers: the evolution of isolated stellar binaries, dynamical capture in dense stellar environments, or yet another channel altogether.

In this paper, we will explore the distribution of binary black hole spins detected by Advanced LIGO and Virgo. Ours is not the first attempt at such an analysis – several authors have previously explored the binary black hole spin distribution, using varying subsets of the LIGO and Virgo detections and employing a range of different models. Our goals in this work are threefold:

1. *Focus on the observable.* Many previous studies aim to describe the distributions of spin magnitudes and/or tilt angles of the individual black holes comprising the observed BBH population (Talbot & Thrane 2017; Farr et al. 2017, 2018; Tiwari et al. 2018; Fernandez & Profumo 2019; Wysocki et al. 2019; Stevenson et al. 2017; Abbott et al. 2019e; Roulet & Zaldarriaga 2019). Gravitational waves carry relatively little information, however, about the spins of these individual components. At leading order, gravitational-wave signals instead depend only on a single effective spin parameter χ_{eff} , quantifying the net projection of both component spins onto a binary’s orbital angular momentum (Damour 2001; Racine 2008; Ajith et al. 2011; Ng et al. 2018; Roulet & Zaldarriaga 2019). We will therefore not attempt to model the ensemble of underlying component spins, but instead seek to describe the more readily-measurable χ_{eff} distribution (Farr et al. 2017, 2018; Tiwari et al. 2018; Roulet & Zaldarriaga 2019).

2. *Adopt a simple population model.* Popular models for the binary black hole spin distribution are often rather complex. The flagship LIGO/Virgo analysis, for example, employs a flexible five-parameter model to describe the ensemble of black hole spins (Abbott et al. 2019e). With only ten detections information these measurements, the resulting constraints from such models are generally uninformative. Here, we will instead adopt a deliberately simple model, characterizing the χ_{eff} distribution via only two parameters: its mean and variance. While this choice sacrifices some flexibility, it will yield transparent and intuitive results that are more robustly extracted from presently small number of gravitational-wave events.

3. *Account for observational biases.* The underlying χ_{eff} distribution is observationally obscured in two ways. The first is selection bias – more highly spinning binary systems accumulate more gravitational-wave cycles, and are thus preferentially detected with higher signal-to-noise ratios. The second is potential measurement degeneracy between effective spin and other binary parameters, most notably the mass ratio (Ng et al. 2018). Previous analyses variously do (Tiwari et al. 2018; Roulet & Zaldarriaga 2019; Abbott et al. 2019e) and do not (Farr et al. 2017, 2018; Fernandez & Profumo 2019) account for these spin-dependent effects.

Just as individual binary black holes inform measurements of the population’s spin distribution, so too can knowledge of the spin distribution inform our conclusions about individual events. After hierarchically measuring the binary black hole χ_{eff} distribution (Sec. 3), we will therefore turn around and use this information

to re-analyze the ten LIGO/Virgo detections, producing updated measurements of their effective spins (Sec. 4).

2. HIERARCHICAL INFERENCE OF BLACK HOLE SPINS

At leading order, the amplitude and phase evolution of a binary’s gravitational-wave signal depend on its component spin through two parameters: the “effective” and “precessing” spins, χ_{eff} and χ_p (Ajith et al. 2011; Schmidt et al. 2015). The effective spin χ_{eff} , a unitless quantity between -1 and 1 , is the mass-weighted average of the dimensionless component spins \vec{a}_1 and \vec{a}_2 , projected along the unit vector \hat{L}_N parallel to the system’s orbital angular momentum:

$$\chi_{\text{eff}} = \frac{(m_1 \vec{a}_1 + m_2 \vec{a}_2) \cdot \hat{L}_N}{m_1 + m_2}. \quad (1)$$

Here, m_i are the source-frame masses of each black hole such that $m_1 > m_2$. The effective spin may also be expressed in terms of the component spin magnitudes a_i and tilt angles t_i between each spin and \hat{L}_N :

$$\chi_{\text{eff}} = \frac{1}{m_1 + m_2} (a_1 m_1 \cos t_1 + a_2 m_2 \cos t_2). \quad (2)$$

χ_p , on the other hand, is a unitless value between 0 and 1 that parametrizes the leading-order effects of orbital precession due to misaligned spins. While χ_{eff} is related to the spin components parallel to \hat{L}_N , χ_p is a linear combination of spin components *normal* to \hat{L}_N .

In this paper, we will focus on understanding the distribution of χ_{eff} across the population of merging stellar-mass black holes. In contrast to more complex, many-parameter models featured in previous work (Abbott et al. 2019e; Wysocki et al. 2019), we will assume that effective spins are drawn from a simple truncated Gaussian,

$$p(\chi_{\text{eff}}|\mu, \sigma^2) = \mathcal{N}(\mu, \sigma^2) \exp\left[\frac{-(\chi_{\text{eff}} - \mu)^2}{2\sigma^2}\right], \quad (3)$$

and to seek to measure the mean μ and variance σ^2 of this ensemble distribution. The normalization constant

$$\mathcal{N}(\mu, \sigma^2) = \sqrt{\frac{2}{\pi\sigma^2}} \left(\text{erf}\left[\frac{1-\mu}{\sqrt{2\sigma^2}}\right] + \text{erf}\left[\frac{1+\mu}{\sqrt{2\sigma^2}}\right] \right)^{-1}. \quad (4)$$

ensures that Eq. (3) is properly normalized over the range $\chi_{\text{eff}} \in [-1, 1]$.

Although χ_{eff} is measured far more precisely than the individual component spins, it is still subject to significant uncertainty (Ng et al. 2018; Abbott et al. 2019a). More specifically, for each gravitational-wave

signal (with associated data d), we do not obtain a direct point estimate of χ_{eff} , but instead a set of discrete samples from the posterior probability distribution $p(\chi_{\text{eff}}|d)$ for the effective spin. We must therefore employ a hierarchical approach in which each LIGO/Virgo BBH event is assumed to have some true but unknown value of χ_{eff} drawn from Eq. (3) above. We will marginalize over the possible χ_{eff} of each LIGO/Virgo event to obtain a posterior on the mean μ and variance σ^2 of the population’s effective spin distribution.

Given N independent binary black hole detections (in our case $N = 10$) with population-averaged detection

efficiency ξ and data $\{d_i\}_{i=1}^N$, the resulting posterior distribution for μ and σ^2 is given in Eq. (5) (Loredo & Wasserman 1995; Loredo 2004; Fishbach et al. 2018; Mandel et al. 2019). The first line corresponds to the ideal case in which the posterior $p(\chi_{\text{eff}}, m_1, m_2, z|d_i)$ on each event’s effective spin, component masses, and redshift z are exactly known; the second line is for the realistic scenario in which we have only discrete samples from the posterior of every event.

$$\begin{aligned}
 p(\mu, \sigma^2 | \{d_i\}_{i=1}^N) &\propto \frac{p(\mu, \sigma^2)}{\xi(\mu, \sigma^2)^N} \prod_{i=1}^N \left[\int d\chi_{\text{eff}} dm_1 dm_2 dz p(\chi_{\text{eff}}, m_1, m_2, z | d_i) \frac{p_{\text{astro}}(m_1, m_2, z)}{p_{\text{pe}}(m_1, m_2, z)} \frac{p(\chi_{\text{eff}} | \mu, \sigma^2)}{p_{\text{pe}}(\chi_{\text{eff}})} \right] \\
 &\propto \frac{p(\mu, \sigma^2)}{\xi(\mu, \sigma^2)^N} \prod_{i=1}^N \left\langle \frac{p_{\text{astro}}(m_{1,j}, m_{2,j}, z_j)}{p_{\text{pe}}(m_{1,j}, m_{2,j}, z_j)} \frac{p(\chi_{\text{eff},j} | \mu, \sigma^2)}{p_{\text{pe}}(\chi_{\text{eff},j})} \right\rangle_{\text{samples } j}
 \end{aligned} \tag{5}$$

The effective spin samples generated by parameter estimation are necessarily obtained under the assumption of some default prior $p_{\text{pe}}(\chi_{\text{eff}})$. The LIGO/Virgo samples produced by the **LALInference** software (Veitch et al. 2015; LIGO Scientific Collaboration 2019), for instance, are given by priors that are uniform in component spin magnitude and orientation, such that $p_{\text{pe}}(a)$ and $p_{\text{pe}}(\cos t)$ are both constant. This corresponds to a symmetric χ_{eff} prior that is broadly peaked about zero. In Eq. (5) we must “undo” this default prior and reweight each sample by the proposed Gaussian distribution $p(\chi_{\text{eff},j} | \mu, \sigma^2)$, evaluated at the given sample value $\chi_{\text{eff},j}$.

LALInference also imposes a computationally-simple but unphysical prior $p_{\text{pe}}(m_1, m_2, z)$ on the component masses and redshift of a binary black hole merger. Specifically, uniform priors are adopted for the *detector* frame masses $m_1(1+z)$ and $m_2(1+z)$ as well as the luminosity distance D_L . This translates into (Abbott et al. 2019e)

$$\begin{aligned}
 p_{\text{pe}}(m_1, m_2, z) \\
 \propto (1+z)^2 D_L(z)^2 \left[D_c(z) + \frac{c(1+z)}{H(z)} \right]. \tag{6}
 \end{aligned}$$

Here, $D_c(z)$ is the comoving distance at redshift z and c is the speed of light. $H(z) = H_0 \sqrt{\Omega_M(1+z)^3 + \Omega_\Lambda}$ is the Hubble parameter, given by the present-day Hubble constant $H_0 = 67.27$ km/s/Mpc and energy densities $\Omega_M = 0.3156$ and $\Omega_\Lambda = 0.6844$ of mass and dark energy, respectively (Ade et al. 2016). Although to-

tal mass $m_1 + m_2$ is not strongly correlated with χ_{eff} , χ_{eff} is generally *anti-correlated* with a binary’s mass ratio $q = m_2/m_1$, as shown in Roulet & Zaldarriaga (2019), for example. The default **LALInference** priors are uniform in detector-frame component masses, and thus preferentially tolerate systems with unequal mass ratios, thereby pushing χ_{eff} posteriors to larger values (Ng et al. 2018; Tiwari et al. 2018). We compensate for this potential bias in Eq. (5) by further reweighting **LALInference** samples by an astrophysically-motivated mass and redshift prior, consistent with the measured mass and redshift distributions of binary black holes following the second Advanced LIGO/Virgo observing run (Abbott et al. 2019e):

$$p_{\text{astro}}(m_1, m_2, z) \propto \frac{(1+z)^{1.7}}{m_1(m_1 - M_{\text{min}})} \frac{dV_c}{dz}. \tag{7}$$

This prior is logarithmically-uniform in primary mass and uniform in mass-ratio, and assumes a binary merger rate that follows star formation, growing as $(1+z)^{2.7}$ in the source frame (Madau & Dickinson 2014). In our detector frame, the measured merger rate is redshifted to $\frac{R(z)}{(1+z)} = (1+z)^{1.7}$. $\frac{dV_c}{dz}$ is the comoving volume per unit redshift, and we assume a minimum black hole mass $M_{\text{min}} = 5 M_\odot$. We do not impose a maximum mass cutoff.

Observational selection effects are accounted for in Eq. (5) by the population-averaged detection efficiency $\xi(\mu, \sigma^2)$, the fraction of all BBH mergers that LIGO suc-

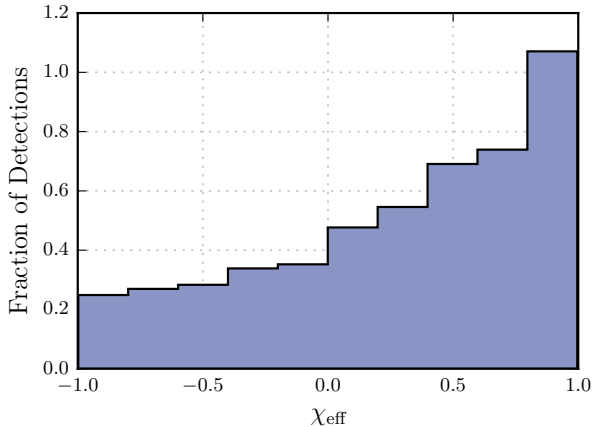


Figure 1. Relative numbers of “detected” synthetic BBHs as a function of χ_{eff} , determined by selecting systems with single-detector matched filter signal-to-noise ratios $\rho \geq 8\sqrt{2}$. The synthetic events have random orientations and sky locations, masses and redshifts following Eq. (7), and effective spins drawn from a uniform distribution between $-1 \leq \chi_{\text{eff}} \leq 1$. Detection probability increases monotonically with χ_{eff} ; at Advanced LIGO’s current sensitivity, a binary with $\chi_{\text{eff}} = 1$ is approximately five times as likely to be detected as one with $\chi_{\text{eff}} = -1$. This distribution of synthetic detections is used in Eq. (9) to mediate the influence of selection effects on the measured χ_{eff} distribution.

cessfully detects:

$$\xi(\mu, \sigma^2) = \int d\chi_{\text{eff}} p(\chi_{\text{eff}} | \mu, \sigma^2) P_{\text{det}}(\chi_{\text{eff}}) \quad (8)$$

where $P_{\text{det}}(\chi_{\text{eff}})$ is the probability, marginalized over all other parameters, that we will detect a BBH with a given χ_{eff} . In practice, we compute $\xi(\mu, \sigma^2)$ via the Monte Carlo approach of Farr (2019), drawing synthetic BBHs with random orientations, masses and redshifts following Eq. (7), and effective spins from a flat reference distribution $p_{\text{ref}}(\chi_{\text{eff}}) \propto 1$. We compute the Advanced LIGO matched filter signal-to-noise ratio ρ for each synthetic BBH using the “Early High-Sensitivity” power spectral density of Abbott et al. (2018b) and the precessing IMRPhenomPv2 waveform model (Hannam et al. 2014), although we assume purely aligned spins. Events with $\rho \geq 8\sqrt{2}$ in the Advanced LIGO detector network are considered to have been “detected.” Figure 1 shows a histogram of the effective spins for these mock detections; at current sensitivities, we see that Advanced LIGO is roughly five times more likely to detect a maximally aligned system ($\chi_{\text{eff}} = 1$) than a maximally anti-aligned system ($\chi_{\text{eff}} = -1$). Given a proposed mean μ and variance σ^2 of the χ_{eff} distribution, the corresponding detection fraction $\xi(\mu, \sigma^2)$ can then be evaluated as a reweighted sum over our catalog of synthetic “detec-

tions” (Farr 2019),

$$\xi(\mu, \sigma^2) = \frac{1}{N_{\text{draw}}} \sum_{i=1}^{N_{\text{det}}} \frac{p(\chi_{\text{eff},i}^{\text{det}} | \mu, \sigma^2)}{p_{\text{ref}}(\chi_{\text{eff},i}^{\text{det}})}, \quad (9)$$

where N_{draw} is the total number of synthetic events, N_{det} is the number of “detections,” and $\chi_{\text{eff},i}^{\text{det}}$ is the effective spin of the i^{th} detected event.

Finally, we note that Eq. (5) does not depend on the overall rate of black hole mergers. As we are concerned only with the *shape* of the χ_{eff} distribution and not the absolute *number* distribution $dN/d\chi_{\text{eff}}$ of mergers, Eq. (5) is derived by marginalizing over the total event rate, assuming a logarithmically uniform rate prior (Fishbach et al. 2018; Mandel et al. 2019).

3. RESULTS FROM O1 AND O2 DETECTIONS

We analyze the ten binary black hole mergers reported by LIGO and Virgo in their O1 and O2 observing runs (Abbott et al. 2019a; LIGO Scientific Collaboration & Virgo Collaboration 2019). Before discussing results, it is useful to review expectations from the literature for the spin distributions resulting from different formation scenarios. Isolated binary evolution is predicted to yield black hole with spins preferentially aligned with their orbit. Although spin misalignments may be introduced by natal supernova kicks, episodes of mass transfer and tidal torques serve to realign component spins before the formation of the final black hole binary (Rodriguez et al. 2016; Zevin et al. 2017; Gerosa et al. 2018; Qin et al. 2018; Zaldarriaga et al. 2018; Bavera et al. 2019). The black holes’ spin *magnitudes* in this scenario are much more uncertain. Recent work indicates that angular momentum is efficiently transported away from stellar cores, leaving black holes with natal spins as low as $a \sim 10^{-2}$ (Qin et al. 2018; Fuller & Ma 2019). While tides on the progenitor of the second-born black hole can spin up the progenitor star (Zaldarriaga et al. 2018), this effect can be counteracted by mass loss in stellar winds, and more detailed simulations find only low or moderate spin increases due to tides (Qin et al. 2018; Bavera et al. 2019). Meanwhile, dynamically-formed systems in dense stellar clusters have no *a priori* preferred axis, and so are likely to have random spin configurations (Rodriguez et al. 2016, 2018; Doctor et al. 2019; Rodriguez et al. 2019). Once again, however, the expected spin magnitudes are largely unknown, subject to the same uncertainties mentioned above regarding natal black hole spins. One firm prediction of the dynamical scenario concerns the spins of *second-generation* binaries, whose components were themselves formed from previous mergers. Regardless

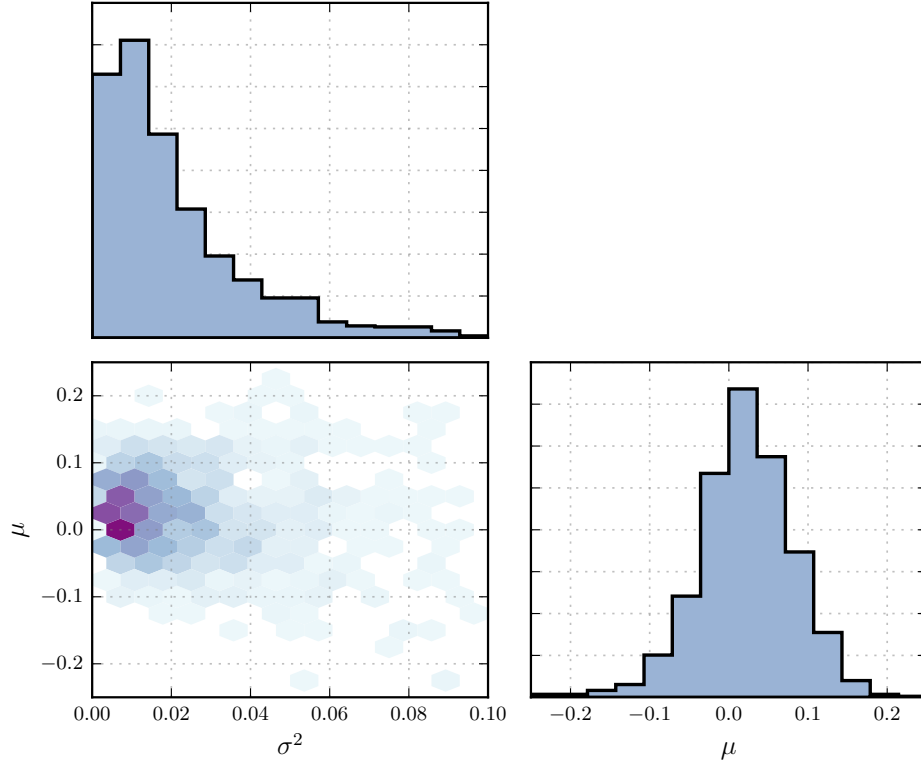


Figure 2. The posterior distributions on the mean μ and variance σ^2 of the χ_{eff} distribution of binary black hole mergers. Given the ten binary black holes observed by Advanced LIGO and Virgo in their first two observing runs, we find $\mu = 0.02^{+0.11}_{-0.13}$ and $\sigma^2 \leq 0.07$ at 95% credibility. Notably, μ remains consistent with zero, as expected for binary black holes formed dynamically in dense stellar environments (Rodríguez et al. 2016, 2018; Doctor et al. 2019; Rodríguez et al. 2019), although isolated binary formation (which would predict $\mu > 0$) remains plausible if black hole spins are intrinsically small (Farr et al. 2017, 2018; Qin et al. 2018; Fuller & Ma 2019). Interestingly, and in contrast to previous results (Roulet & Zaldarriaga 2019), we find that σ^2 is consistent with 0; we therefore cannot rule out an arbitrarily narrow χ_{eff} distribution.

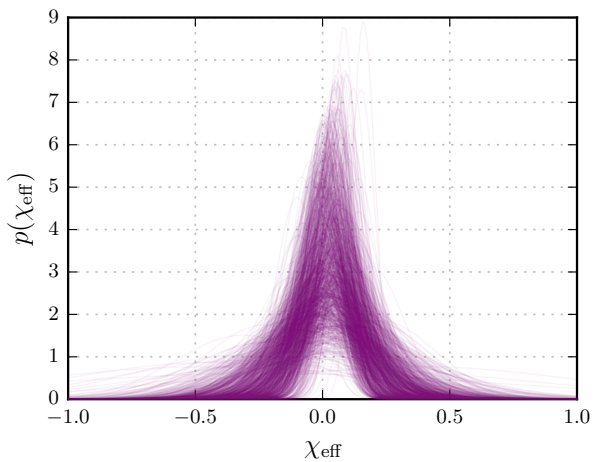


Figure 3. A superposition of the allowed Gaussian χ_{eff} distributions corresponding to the (μ, σ^2) samples shown in Fig. 2. The known population of binary black holes robustly requires a χ_{eff} distribution that is narrowly peaked about zero. We do, however, see a slight preference for positive χ_{eff} , as previously shown in Fig. 2.

of their component spins, black hole mergers generally yield remnants with $a \sim 0.7$; thus the effective spin of two such second-generation binaries may be large (Fishbach et al. 2017; Gerosa & Berti 2017; Rodríguez et al. 2018; Doctor et al. 2019; Rodríguez et al. 2019).

In summary, the most robust discriminator between the isolated binary and dynamical scenarios is the mean μ of the effective spin distribution. If isolated binaries have preferentially aligned spins, then we expect an effective spin distribution centered on a positive value: $\mu > 0$. Dynamically-formed binaries with random spin orientations, meanwhile, should have a symmetric χ_{eff} distribution centered at $\mu = 0$ (Farr et al. 2018).

To generate our posterior distributions for μ and σ^2 , we sample from Eq. 5 using `emcee`, a Markov Chain Monte Carlo (MCMC) package in Python (Foreman-Mackey et al. 2013). We use the public `LALInference` samples made available through the Gravitational Wave Open Science Center (Vallisneri et al. 2015; LIGO Scientific Collaboration & Virgo Collaboration 2019). Specifically, we use the so-called “overall posterior”

samples, which are a union of the samples obtained with the IMRPhenomPv2 (Hannam et al. 2014) and SEOBNRv3 (Taracchini et al. 2014; Pan et al. 2014) waveform models; we have confirmed that our results are robust under the use of either waveform model independently. We adopt flat priors across the ranges $\mu \in [-1, 1]$ and $\sigma^2 \in [0, 1]$. Our posterior on μ and σ^2 is given in Fig. 2. With the ten binary black holes observed in O1 and O2 by Advanced LIGO and Virgo, we constrain the mean of the binary black hole χ_{eff} distribution to $\mu = 0.02^{+0.11}_{-0.13}$. Hence we find no evidence for preferential spin alignment, which would manifest as preferentially positive μ . Meanwhile, we find that width of the χ_{eff} distribution must be extremely small, with a variance $\sigma^2 < 0.07$ at 95% credibility. Curiously, provided that μ is nonzero, the data are consistent with a vanishingly narrow spin distribution. This can be seen in Fig. 2, which does not exclude $\sigma^2 = 0$. We therefore cannot yet rule out the possibility that the χ_{eff} distribution is a delta function, with all binary black holes sharing the same effective spin value.

In Fig. 3, we plot the ensemble of permitted χ_{eff} distributions consistent with our posterior on μ and σ^2 . This figure again shows our slight preference for positive μ , but primarily illustrates that all χ_{eff} distributions consistent with the presently-known binary black hole mergers must be narrowly peaked about ~ 0 .

Such small effective spins likely indicate one of three possibilities. First, these results are compatible with a scenario in which component spins are large but preferentially lie in the plane perpendicular to the binary’s orbital angular momentum. Intriguingly, some models for binary mergers driven by Kozai-Lidov resonances (Kozai 1962; Lidov 1962) in hierarchical triples predict preferentially perpendicular spins (Rodriguez & Antonini 2018; Antonini et al. 2018; Liu & Lai 2018), although this effect is not observed in all studies (Antonini et al. 2018; Liu et al. 2019). Second, all component spins could be large but primarily anti-aligned with one another, such that each spin cancels the other’s contribution to Eq. (1); we are not aware of any merger channels that predict this. (Note, however, that BBH formation in the disks of active galactic nuclei may lead to the unique possibility of anti-aligned spins in approximately *half* of the BBH population (McKernan et al. 2019; Yang et al. 2019)). Finally, as has been noted by other authors, these results may point to the simple fact that binary black hole component spins are intrinsically small (Farr et al. 2017; Tiwari et al. 2018; Wysocki et al. 2019). This final scenario would yield a χ_{eff} distribution concentrated around zero, regardless of spin orientation. By positing small natal spins, models of isolated field bina-

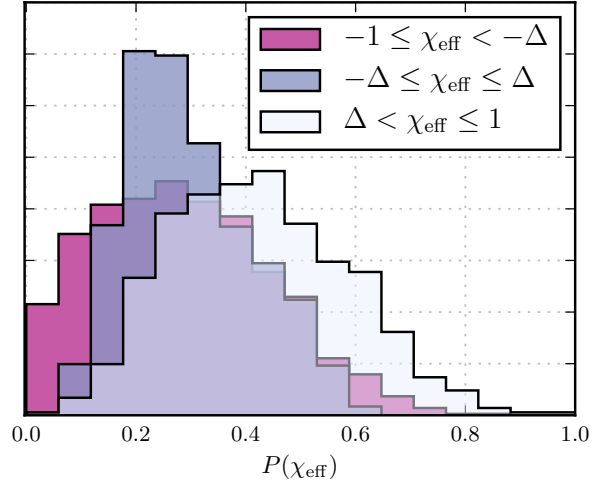


Figure 4. Histogram of the probability that there exists binary black holes with various effective spins χ_{eff} . Here, $\Delta = 0.05$, representing a minimal detectable χ_{eff} value (Farr et al. 2018; Abbott et al. 2019e). The data represents the area under each distribution plotted in Fig. 3, for each χ_{eff} range indicated. If the ten LIGO/Virgo binary black hole detections are a representative draw from the local universe’s BBH population, then these results indicate that in future detections, positive χ_{eff} is more likely to be observed than negative χ_{eff} . Notice that the negative χ_{eff} histogram includes 0 while the other two do not.

ries (Belczynski et al. 2017; Postnov & Kuranov 2019), dynamical formation (Rodriguez et al. 2019), and hierarchical triples (Antonini et al. 2018) can all produce distributions like those shown in Fig. 3.

Given the theoretical uncertainties in spin magnitude, some authors have suggested that, rather than μ and σ^2 , a more robust prediction might be the *fraction* of black hole binaries with negative χ_{eff} (Rodriguez et al. 2016; Gerosa et al. 2018). In Fig. 4, we show posteriors on the fractions of binaries with positive and negative effective spins. We follow Farr et al. (2018) and Abbott et al. (2019e) in additionally defining a third “uninformative” bin $-\Delta \leq \chi_{\text{eff}} \leq \Delta$, with $\Delta = 0.05$, in which effective spins are essentially indistinguishable from zero. At 95% credibility, a fraction $0.28^{+0.26}_{-0.17}$ of binaries are expected to have uninformatively small effective spins. Of the informative events, $0.41^{+0.38}_{-0.37}$ are predicted to have negative spins. Notably, however, the posteriors in Fig. 4 do not exclude the possibility of *no* detectably-negative effective spins; instead we can only confidently limit the fraction of detectably negative effective spins to ≤ 0.75 at 95% credibility. These results differ from Abbott et al. (2019e), which reports that $\sim 80\%$ of BBH have uninformatively small spins. This difference can be attributed to two possibilities.

First, if the true χ_{eff} distribution is narrower than we can presently resolve with 10 events, then our Gaussian model will generally overestimate the width of the χ_{eff} distribution, thereby *underestimating* the fraction of uninformative events. Alternatively, if the width of the true χ_{eff} distribution is comparable to or larger than Δ , then the piecewise “three-bin” model of Farr et al. (2018) and Abbott et al. (2019e) is a poor representation of the true underlying distribution, and will generally *overestimate* the fraction of uninformative events in the central bin. We may be seeing the effects of one or both of these possibilities, since they are not mutually exclusive.

It is worth noting that Roulet & Zaldarriaga (2019) have also explored a Gaussian model for the binary black hole χ_{eff} distribution, obtaining constraints on μ consistent with ours when analyzing the GWTC-1 catalogue. Our measurement of σ^2 , however, qualitatively differs from their results. Where our posterior permits extremely small σ^2 , Roulet & Zaldarriaga (2019)’s results exclude a vanishingly narrow χ_{eff} distribution. This distinction could be due to a number of differences between our two analyses. First, while both analyses adopt a uniform prior in mass ratio, Roulet & Zaldarriaga (2019) additionally assume a uniform prior in chirp mass, while our prior is logarithmically uniform in primary mass. We have verified, though, that the adoption of a uniform-in-chirp-mass prior does not affect our results. Second, perhaps more significantly, to generate posteriors on μ and σ^2 , Roulet & Zaldarriaga (2019) rely on analytic likelihood evaluations performed under a number of simplifying assumptions, such as the perfect alignment of all component spins. On the other hand, we use posterior distributions sampled by MCMC methods. Finally, Roulet & Zaldarriaga (2019) evaluate the detection efficiency $\xi(\mu, \sigma^2)$ via direct integra-

tion, whereas again we take a Monte Carlo approach as described above. A consequence of our Monte Carlo method is that, numerically speaking, we cannot sample arbitrarily close to $\sigma^2 = 0$. As σ^2 approaches zero, the detection efficiency $\xi(\mu, \sigma^2)$ vanishes and the likelihood diverges to infinity. To prevent this divergence, we impose the stability condition recommended in Farr (2019) – that the number of synthetic detections contributing to Eq. (9) be greater than $4N$ (where $N = 10$ is our number of real events). This condition prevents us from sampling variances below $\sigma^2 \leq 0.03$; even at $\sigma^2 = 0.03$, though, our posterior remains flat.

4. REFINED BINARY BLACK HOLE SPIN MEASUREMENTS

Given what we now know about the population distribution of χ_{eff} , we can obtain refined χ_{eff} measurements on each individual binary black hole system. As described in Sec. 2, the default **LALInference** priors on component spins are uniform in dimensionless magnitude and isotropic in direction. Having obtained information about the actual population distribution of χ_{eff} , we can replace the uninformative **LALInference** prior with one that matches the recovered χ_{eff} distribution. Specifically, we will recompute the posterior $p(\chi_{\text{eff}}|d)$ on the effective spin of each of the ten binary black hole detections, marginalizing over all possible values of μ and σ^2 . We will additionally undo the default **LALInference** mass and redshift priors, reweighting by our astrophysically-motivated prior in Eq. (7).

For brevity, we’ll introduce the abbreviation $\lambda = \{\chi_{\text{eff}}, m_1, m_2, z\}$ for the set of parameters describing an individual compact binary. Given the complete set $D = \{d_i\}_{i=1}^N$ for all our $N = 10$ events, we can form a joint posterior on μ, σ^2 , and the parameters λ of some *single* event:

$$p(\lambda, \mu, \sigma^2 | D) \propto p(\lambda | d) \frac{p(\lambda | \mu, \sigma^2)}{p_{\text{pe}}(\lambda)} \left(\frac{p(\mu, \sigma^2)}{\xi(\mu, \sigma^2)^N} \prod_{i=1}^{N-1} \left[\int d\lambda \, p(\lambda | d_i) \frac{p(\lambda | \mu, \sigma^2)}{p_{\text{pe}}(\lambda)} \right] \right). \quad (10)$$

This is simply Eq. (5), absent marginalization over the single event of interest. Equation (10) can be put into a more convenient form if we multiply and divide by $p(d|\mu, \sigma^2) = \int d\lambda \, p(\lambda | d) \frac{p(\lambda | \mu, \sigma^2)}{p_{\text{pe}}(\lambda)}$. This gives

$$\begin{aligned} p(\lambda, \mu, \sigma^2 | D) &\propto \frac{p(\lambda | d)}{p(d | \mu, \sigma^2)} \frac{p(\lambda | \mu, \sigma^2)}{p_{\text{pe}}(\lambda)} \left(\frac{p(\mu, \sigma^2)}{\xi(\mu, \sigma^2)^N} \prod_{i=1}^N \left[\int d\lambda_i \, p(\lambda_i | d_i) \frac{p(\lambda_i | \mu, \sigma^2)}{p_{\text{pe}}(\lambda_i)} \right] \right) \\ &\propto \frac{p(\lambda | d)}{p(d | \mu, \sigma^2)} \frac{p(\lambda | \mu, \sigma^2)}{p_{\text{pe}}(\lambda)} p(\mu, \sigma^2 | D). \end{aligned} \quad (11)$$

This expression now depends only on the default posterior $p(\lambda | d)$ for the event of interest and the marginal pos-

terior $p(\mu, \sigma^2 | D)$ on the population parameters given *all* N events – exactly what we computed above in Sect. 2.

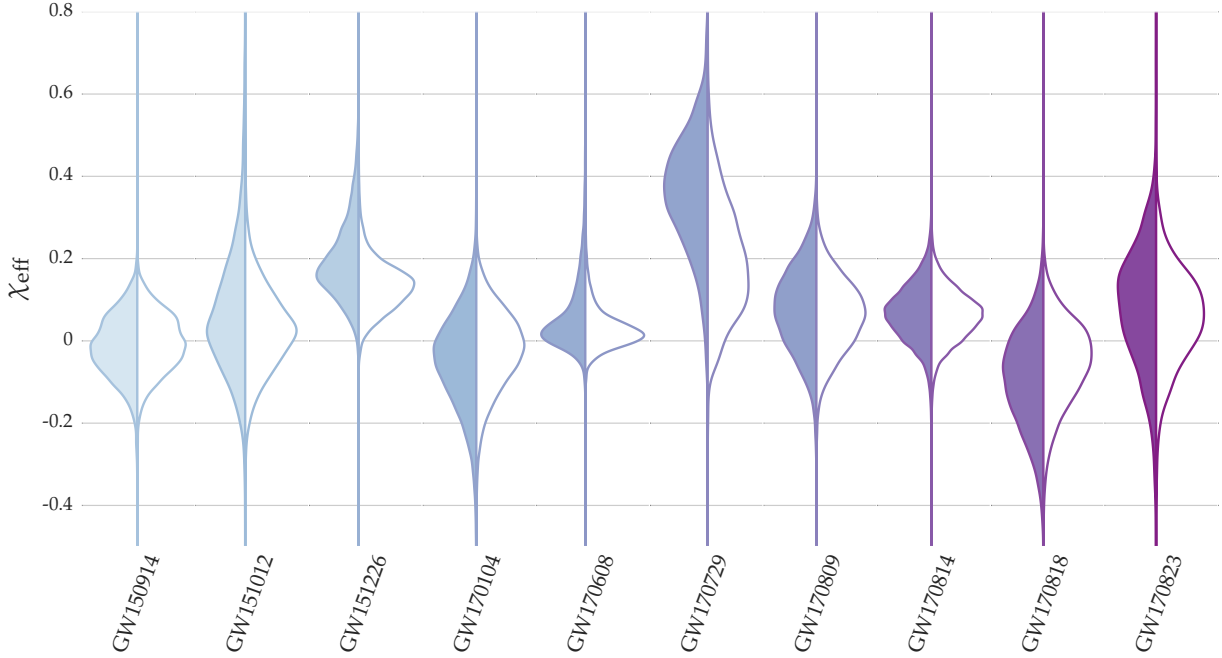


Figure 5. Violin plot showing the posterior distribution on χ_{eff} under the **LALInference** χ_{eff} prior (filled in) and the population-distribution-informed prior (white) for each binary black hole event. The **LALInference** prior for spin is uniform in spin magnitude and isotropic in spin tilt angle. The colors in this plot are used to distinguish between events, which are plotted in order of detection date. Notice that the population-distribution-informed prior brings each posterior distribution closer to $\chi_{\text{eff}} = 0$. This means that when the spin distribution of the binary black hole population is not used to inform parameter estimation, we consistently overestimate the magnitude of χ_{eff} .

Given discrete samples from $p_{\text{pe}}(\chi_{\text{eff}}, m_1, m_2, z|d)$ and $p(\mu, \sigma^2|D)$, we can sample Eq. (10) via a two step procedure, in which we (i) select a posterior sample $\{\mu_i, \sigma_i^2\}$ from $p(\mu, \sigma^2|D)$, then (ii) select a random parameter estimation sample $\lambda_j \equiv \{\chi_{\text{eff}}, m_1, m_2, z\}_j$, subject to the weights

$$w_j = \frac{p(\lambda_j|\mu_i, \sigma_i^2)}{p_{\text{pe}}(\lambda_j)} = \frac{p(\chi_{\text{eff},j}|\mu_i, \sigma_i^2) p(m_{1,j}, m_{2,j}, z_j)}{p_{\text{pe}}(\chi_{\text{eff},j}) p_{\text{pe}}(m_{1,j}, m_{2,j}, z_j)}. \quad (12)$$

Equation (11) contains an extra factor, $p(d|\mu, \sigma^2)^{-1}$, that does not appear in the above weights. This is because, once we condition on the particular values μ_i and σ_i^2 , the factor $p(d|\mu, \sigma^2)$ appearing in Eq. (11) is a constant; we can therefore neglect it from the weights in Eq. (12).

For each of the ten binary black holes detected in O1 and O2 by Advanced LIGO Virgo, Fig. 5 compares the default **LALInference** χ_{eff} posteriors to our population-informed posteriors. The **LALInference** posteriors are shaded, while the population-informed posteriors are in white. In all cases the population-informed prior serves to shift each posterior distribution towards $\chi_{\text{eff}} = 0$. This shift operates in both directions – posteriors that

strongly support positive χ_{eff} are moved downward, while posteriors supporting negative effective spins shift up. This “shrinkage” effect is common to hierarchical models of observations with significant uncertainty (Lieu et al. 2017). GW170729, for example, excludes $\chi_{\text{eff}} \leq 0$ with 99% credibility when using uninformative priors. The population-informed prior, though, noticeably shifts the GW170729’s χ_{eff} posterior downward; 8% of the posterior now extends below $\chi_{\text{eff}} = 0$ and the peak is lowered from $\chi_{\text{eff}} \approx 0.4$ to 0.1. The effective spin of GW151226, on the other hand, remains confidently positive, with $\chi_{\text{eff}} > 0$ at 99% credibility under both the uninformative and population-informed priors. GW170818, meanwhile, originally shows moderate support for negative effective spins, with 77% of the posterior at $\chi_{\text{eff}} < 0$. Under our population-informed prior, 68% of GW170818’s χ_{eff} prior now supports negative values.

A key takeaway from these results is that when a collection of binary black holes are analyzed in isolation under default priors common to such analyses, the magnitude of their effective spins will be consistently overestimated. When studying future compact binary mergers, it will be essential to evaluate their spins in the context of the broader population, particularly when an

event seemingly has confidently positive or negative χ_{eff} . Further updated population-informed posteriors on the parameters of individual gravitational wave events are given in Fishbach et al. (2019) and Galaudage et al. (2019).

5. CONCLUSION

As we enter deeper into the era of gravitational-wave astronomy, increasingly valuable information will be encoded in the ensemble properties of compact binary mergers. The distribution of parameters like mass, spin, and redshift across the observable universe’s binary black hole population contain essential information about the formation and evolutionary pathways of such systems. We focus on the population distribution for effective spin, χ_{eff} . This parameter characterizes gravitational-wave strain at leading order, and is thus easily accessible from the data from the small number of LIGO/Virgo events. Additionally, our focus on this single phenomenological parameter provides a simple and intuitive framework on which future analyses can be built. In a complementary paper, for example, Safarzadeh et al. (2020) extend our model to investigate correlations between the effective spins and masses of binary black holes.

In this paper, we have explored the distribution of the effective spin parameter χ_{eff} across the ten binary black holes observed by LIGO and Virgo in their O1 and O2 observing run. We adopted a simple and intuitive model, measuring the mean μ and variance σ^2 of effective spins across this ensemble of gravitational-wave events, and rigorously accounting for observational selection effects and degeneracies. At 95% credibility, we found $\mu = 0.02^{+0.11}_{-0.13}$ and $\sigma^2 \leq 0.07$. Notably, σ^2 is consistent with 0, meaning that the distribution of BBH effective spins is consistent with a delta function. As discussed in Sec. 3, it is not clear whether this result preferentially supports a dynamical or field binary origin (or even other possibilities) for stellar-mass binary black holes. Instead, this result likely indicates that binary black holes have small spin magnitudes, far

smaller than those inferred in x-ray binaries (Miller & Miller 2015).

Our knowledge of the ensemble distribution of χ_{eff} , in turn, allowed us to refine χ_{eff} measurements for individual binary black hole events. Existing spin measurements were obtained under an uninformative prior on component spin magnitudes and orientations. Here, we instead used our measurements of μ and σ^2 to generate a *population-informed* prior, which we used to reweight existing parameter estimation results for the ten O1 and O2 binary black hole detections. Using our population-informed prior, the resulting effective spin posteriors are all shifted towards $\chi_{\text{eff}} = 0$. In some cases this shift is significant. For example, GW170729 previously excluded $\chi_{\text{eff}} = 0$ at 99% credibility. Under a population-informed prior, however, it shows a $\sim 10\%$ probability for zero (or negative) effective spin. More broadly, our results demonstrate the value of analyzing the ensemble of binary black holes in unison; when treating each binary black hole in isolation, we will consistently overestimate the magnitude (positive or negative) of χ_{eff} .

ACKNOWLEDGEMENTS

We would like to thank Christopher Berry, Thomas Dent, Zoheyr Doctor, Maya Fishbach, and others within the LIGO Scientific Collaboration and Virgo Collaboration for constructive comments and helpful conversation. The Flatiron Institute is supported by the Simons Foundation. This research has made use of data, software and/or web tools obtained from the Gravitational Wave Open Science Center (<https://www.gwopenscience.org>), a service of LIGO Laboratory, the LIGO Scientific Collaboration and the Virgo Collaboration. LIGO is funded by the U.S. National Science Foundation. Virgo is funded by the French Centre National de Recherche Scientifique (CNRS), the Italian Istituto Nazionale della Fisica Nucleare (INFN) and the Dutch Nikhef, with contributions by Polish and Hungarian institutes.

REFERENCES

- Aasi, J., Abbott, B. P., Abbott, R., et al. 2015, Classical and Quantum Gravity, 32, 074001
- Abbott, B. P., Abbott, R., Abbott, T. D., et al. 2016a, Phys. Rev. X, 6, 041015. <https://link.aps.org/doi/10.1103/PhysRevX.6.041015>
- . 2016b, Phys. Rev. Lett., 116, 241102
- . 2016c, Phys. Rev. Lett., 116, 221101. <https://link.aps.org/doi/10.1103/PhysRevLett.116.221101>
- . 2017, Phys. Rev. Lett., 119, 161101. <https://link.aps.org/doi/10.1103/PhysRevLett.119.161101>
- . 2018a, Phys. Rev. Lett., 121, 161101. <https://link.aps.org/doi/10.1103/PhysRevLett.121.161101>
- . 2018b, Living Reviews in Relativity, 21, 3
- . 2019a, Phys. Rev. X, 9, 031040
- . 2019b, Physical Review X, 9, 011001

- . 2019c, *Phys. Rev. Lett.*, 123, 011102. <https://link.aps.org/doi/10.1103/PhysRevLett.123.011102>
- . 2019d, arXiv e-prints, arXiv:1903.04467
- . 2019e, *Astrophys. J. Lett.*, 882, L24
- Acernese, F., Agathos, M., Agatsuma, K., et al. 2015, *Classical and Quantum Gravity*, 32, 024001
- Ade, P. A. R., Aghanim, N., Arnaud, M., et al. 2016, *Astronomy & Astrophysics*, 594, A13. <http://dx.doi.org/10.1051/0004-6361/201525830>
- Ajith, P., Hannam, M., Husa, S., et al. 2011, *Phys. Rev. Lett.*, 106, 241101
- Antonini, F., Rodriguez, C. L., Petrovich, C., & Fischer, C. L. 2018, *Monthly Notices of the Royal Astronomical Society: Letters*, 480, L58. <https://academic.oup.com/mnrasl/article/480/1/L58/5053071>
- Aso, Y., Michimura, Y., Somiya, K., et al. 2013, *Physical Review D*, 88, 043007. <http://link.aps.org/doi/10.1103/PhysRevD.88.043007>
- Bavera, S. S., Fragos, T., Qin, Y., et al. 2019, arXiv:1906.12257 [astro-ph], arXiv: 1906.12257. <http://arxiv.org/abs/1906.12257>
- Belczynski, K., Klencki, J., Fields, C. E., et al. 2017, arXiv e-prints, arXiv:1706.07053
- Chatziioannou, K., Cotesta, R., Ghonge, S., et al. 2019, arXiv e-prints, arXiv:1903.06742
- Damour, T. 2001, *PhRvD*, 64, 124013
- Doctor, Z., Wysocki, D., O’Shaughnessy, R., Holz, D. E., & Farr, B. 2019, arXiv:1911.04424 [astro-ph], arXiv: 1911.04424. <http://arxiv.org/abs/1911.04424>
- Farr, B., Holz, D. E., & Farr, W. M. 2018, *ApJL*, 854, L9
- Farr, W. M. 2019, *Research Notes of the American Astronomical Society*, 3, 66
- Farr, W. M., Stevenson, S., Miller, M. C., et al. 2017, *Nature*, 548, 426
- Fernandez, N., & Profumo, S. 2019, *JCAP*, 2019, 022
- Fishbach, M., Farr, W. M., & Holz, D. E. 2019, arXiv e-prints, arXiv:1911.05882
- Fishbach, M., Holz, D. E., & Farr, B. 2017, *Astrophys. J.*, 840, L24
- Fishbach, M., Holz, D. E., & Farr, W. M. 2018, *Astrophys. J. Lett.*, 863, L41
- Foreman-Mackey, D., Hogg, D. W., Lang, D., & Goodman, J. 2013, *PASP*, 125, 306
- Fuller, J., & Ma, L. 2019, *ApJL*, 881, L1
- Galaudage, S., Talbot, C., & Thrane, E. 2019, arXiv e-prints, arXiv:1912.09708
- Gerosa, D., & Berti, E. 2017, *PhRvD*, 95, 124046
- Gerosa, D., Berti, E., O’Shaughnessy, R., et al. 2018, *Physical Review D*, 98, 084036. <https://link.aps.org/doi/10.1103/PhysRevD.98.084036>
- Hannam, M., Schmidt, P., Boh, A., et al. 2014, *Phys. Rev. Lett.*, 113, 151101
- Kimball, C., Berry, C. P. L., & Kalogera, V. 2019, arXiv e-prints, arXiv:1903.07813
- Kozai, Y. 1962, *The Astronomical Journal*, 67, 591. http://adsabs.harvard.edu/cgi-bin/bib_query?1962AJ.....67..591K
- Lidov, M. L. 1962, *PLANSS*, 9, 719
- Lieu, M., Farr, W. M., Betancourt, M., et al. 2017, *MNRAS*, 468, 4872
- LIGO Scientific Collaboration. 2019, *LIGO Algorithm Library - LALSuite*, Free software (GPL), git.ligo.org, doi:10.7935/GT1W-FZ16
- LIGO Scientific Collaboration & Virgo Collaboration. 2019, *Parameter Estimation Sample Release for GWTC-1*, Gravitational Wave Open Science Center, doi:https://doi.org/10.7935/KSX7-QQ51
- Liu, B., & Lai, D. 2018, *The Astrophysical Journal*, 863, 68. <http://stacks.iop.org/0004-637X/863/i=1/a=68?key=crossref.adc80f31c47f26f0d62f8a05afc6a048>
- Liu, B., Lai, D., & Wang, Y.-H. 2019, *The Astrophysical Journal*, 881, 41. <https://iopscience.iop.org/article/10.3847/1538-4357/ab2dfb>
- Loredo, T. J. 2004, in *American Institute of Physics Conference Series*, Vol. 735, American Institute of Physics Conference Series, ed. R. Fischer, R. Preuss, & U. V. Toussaint, 195–206
- Loredo, T. J., & Wasserman, I. M. 1995, *Astrophys. J. Supplement*, 96, 261
- Madau, P., & Dickinson, M. 2014, *Annual Review of Astronomy and Astrophysics*, 52, 415. <http://www.annualreviews.org/doi/10.1146/annurev-astro-081811-125615>
- Mandel, I., Farr, W. M., & Gair, J. R. 2019, *Mon. Not. R. Astron. Soc.*, 486, 1086
- McKernan, B., Ford, K. E. S., O’Shaughnessy, R., & Wysocki, D. 2019, arXiv e-prints, arXiv: 1907.04356
- Miller, M. C., & Miller, J. M. 2015, *PhR*, 548, 1
- Ng, K. K. Y., Vitale, S., Zimmerman, A., et al. 2018, *Phys. Rev. D*, 98, 083007
- Pan, Y., Buonanno, A., Taracchini, A., et al. 2014, *PhRvD*, 89, 084006
- Postnov, K. A., & Kuranov, A. G. 2019, *MNRAS*, 483, 3288
- Qin, Y., Fragos, T., Meynet, G., et al. 2018, *Astronomy & Astrophysics*, 616, A28. <https://www.aanda.org/10.1051/0004-6361/201832839>
- Racine, É. 2008, *PhRvD*, 78, 044021
- Raithel, C. A., Özel, F., & Psaltis, D. 2018, *Astrophys. J. Lett.*, 857, L23

- Rodriguez, C. L., Amaro-Seoane, P., Chatterjee, S., & Rasio, F. A. 2018, *Physical Review Letters*, 120, 151101. <https://link.aps.org/doi/10.1103/PhysRevLett.120.151101>
- Rodriguez, C. L., & Antonini, F. 2018, *The Astrophysical Journal*, 863, 7. <http://stacks.iop.org/0004-637X/863/i=1/a=7?key=crossref.b5f511c3e797a7d9bd2e93e68431b14d>
- Rodriguez, C. L., Zevin, M., Amaro-Seoane, P., et al. 2019, *Physical Review D*, 100, 043027. <https://link.aps.org/doi/10.1103/PhysRevD.100.043027>
- Rodriguez, C. L., Zevin, M., Pankow, C., Kalogera, V., & Rasio, F. A. 2016, *The Astrophysical Journal*, 832, L2. <http://stacks.iop.org/2041-8205/832/i=1/a=L2?key=crossref.4596eb16407534b60744e1ce84ff1198>
- Roulet, J., & Zaldarriaga, M. 2019, *Monthly Notices of the Royal Astronomical Society*, 484, 4216. <https://academic.oup.com/mnras/article/484/3/4216/5298900>
- Safarzadeh, M., Farr, W. M., & Ramirez-Ruiz, E. 2020, arXiv e-prints, arXiv:2001.06490
- Schmidt, P., Ohme, F., & Hannam, M. 2015, *Phys. Rev. D*, 91, 024043
- Stevenson, S., Berry, C. P. L., & Mandel, I. 2017, *Mon. Not. R. Astron. Soc.*, 471, 2801
- Talbot, C., & Thrane, E. 2017, *Phys. Rev. D*, 96, 023012
- Taracchini, A., et al. 2014, *Phys. Rev.*, D89, 061502
- Tiwari, V., Fairhurst, S., & Hannam, M. 2018, *Astrophys. J.*, 868, 140
- Vallisneri, M., Kanner, J., Williams, R., Weinstein, A., & Stephens, B. 2015, in *Journal of Physics Conference Series*, Vol. 610, *Journal of Physics Conference Series*, 012021
- Veitch, J., Raymond, V., Farr, B., et al. 2015, *Phys. Rev. D*, 91, 042003
- Wysocki, D., Lange, J., & O’Shaughnessy, R. 2019, *Phys. Rev. D*, 100, 043012. <https://link.aps.org/doi/10.1103/PhysRevD.100.043012>
- Yang, Y., Bartos, I., Gayathri, V., et al. 2019, *PhRvL*, 123, 181101
- Zaldarriaga, M., Kushnir, D., & Kollmeier, J. A. 2018, *Monthly Notices of the Royal Astronomical Society*, 473, 4174. <http://academic.oup.com/mnras/article/473/3/4174/4349758>
- Zevin, M., Pankow, C., Rodriguez, C. L., et al. 2017, *The Astrophysical Journal*, 846, 82. <http://stacks.iop.org/0004-637X/846/i=1/a=82?key=crossref.727554ae4227b94fd675b5260474b841>